

Three-dimensional quantum Griffiths singularity in bulk iron-pnictide superconductors

Shao-Bo Liu^{1†}, Congkuan Tian^{1,2†}, Yongqing Cai^{3,4†}, Hang Cui¹, Xinjian Wei², Mantang Chen¹, Yang Zhao¹, Yuan Sui¹, Shuyue Guan¹, Shuang Jia¹, Yu Zhang², Ya Feng², Jiankun Li², Jian Cui², Yuanjun Song², Tingting Hao², Chaoyu Chen⁴, Jian-Hao Chen^{1,2,5,6*}

¹ International Center for Quantum Materials, School of Physics, Peking University, Beijing 100091, China

² Beijing Academy of Quantum Information Sciences, Beijing 100094, China

³ School of Physics, Dalian University of Technology, Dalian 116024, China

⁴ Shenzhen Institute for Quantum Science and Engineering and Department of Physics, Southern University of Science and Technology, Shenzhen 518055, China.

⁵ Key Laboratory for the Physics and Chemistry of Nanodevices, Peking University, Beijing 100091, China

⁶ Hefei National Laboratory, Hefei 230026, China

[†]These authors contributed equally to this work.

Corresponding Author:

*E-mail: Jian-Hao Chen (chenjianhao@pku.edu.cn)

Abstract

The quantum Griffiths singularity (QGS) is a phenomenon driven by quenched disorders that break conventional scaling invariance and result in a divergent dynamical critical exponent during quantum phase transitions (QPT). While this phenomenon has been well-documented in low-dimensional conventional superconductors and in three-dimensional (3D) magnetic metal systems, its presence in 3D superconducting systems and in unconventional high-temperature superconductors (high- T_c SCs) remains unclear. In this study, we report the observation of robust QGS in the superconductor-metal transition (SMT) of both quasi-2D and 3D anisotropic unconventional high- T_c superconductor $\text{CaFe}_{1-x}\text{Ni}_x\text{AsF}$ ($x < 5\%$) bulk single crystals, where the QGS states persist to up to 5.3 K. A comprehensive quantum phase diagram is established that delineates the 3D anisotropic QGS of SMT induced by perpendicular and parallel magnetic field. Our findings reveal the universality of QGS in 3D superconducting systems and unconventional high- T_c SCs, thereby substantially expanding the range of applicability of QGS.

Introduction

The superconductor-insulator (metal) transition (SIT/SMT), a prototypical example of quantum phase transition (QPT), has garnered significant attention due to its implications for understanding quantum states of matter as well as its potential applications in novel low-dimensional superconducting quantum computing devices¹⁻⁷. In conventional SIT/SMT systems, a single quantum critical point (QCP) with power-law divergence of a single spatial or temporal correlation length as a function of non-thermal control parameters is presented^{2,8,9}. The critical exponents of the divergence reflect the universality class of the quantum critical behavior^{10,11}. However, the presence of quenched disorders can disrupt conventional scaling invariance and alter the universality class of the QPT, leading to the emergence of the quantum Griffiths phase, which is characterized by continuously varying critical exponents with respect to temperature and control parameters, fundamentally challenging the conventional understanding of QPT in homogeneous disordered systems¹²⁻¹⁶. In the quantum Griffiths phase, distinct superconducting islands ("rare regions") emerge and the fluctuations of the order parameter within these rare regions become non-negligible¹²⁻¹⁶. QGS have been experimentally observed in two-dimensional (2D)^{5,17-23} and quasi-one-dimensional (quasi-1D)⁷ conventional superconductors. However, the fate of QGS in three-dimensional bulk superconductors and unconventional high- T_c superconductors remains unknown.

The 1111-type FeAs-based superconductors are the earliest discovered iron-based unconventional high- T_c superconductors with the highest T_c in the material family²⁴. CaFeAsF, a representative parent compound of the 1111-type FeAs-based superconductors, is an antiferromagnetic bad-metal consisting of alternately stacked CaF and FeAs layers along the c -axis²⁴. Quantum oscillation measurements in CaFeAsF, along with band-structure calculations, revealed a pair of symmetry-related Dirac electron cylinders and a normal hole cylinder at the Fermi surface²⁵. Nontrivial topological electronic structure has been predicted in CaFeAsF arising from strong electronic correlations of the Fe 3d electrons²⁶ and superconductivity in CaFeAsF can be achieved through chemical doping or external pressure^{24,27,28}. Although undoped CaFeAsF is not superconducting at ambient pressure, a magnetic-field-induced metal-insulator QPT near the

quantum limit has been reported²⁹, providing a plausible precursor for SIT/SMT in doped and superconducting CaFeAsF. Electron doping of CaFeAsF can be achieved by substituting a fraction of Fe with Ni, resulting in the formation of CaFe_{1-x}Ni_xAsF ($x \ll 1$). However, single crystal of CaFe_{1-x}Ni_xAsF has been challenging to grow, impeding further exploration of this material.

In this study, superconducting single crystals of CaFe_{1-x}Ni_xAsF ($x < 5\%$) is successfully synthesized using the flux method (details in Methods and Supplementary Information S1 and S2). In all the samples where SMTs are realized, multiple QCPs and diverging dynamic critical exponents are observed, providing direct evidence of QGS in these materials^{5,12,18,30}. By fitting the experimental divergence behavior of "critical exponent" versus magnetic field to an activated scaling law⁵, the value of the extracted exponents are 0.6 and 0.4 for quasi-2D and 3D anisotropic CaFe_{1-x}Ni_xAsF, respectively, consistent with theoretical predictions and numerical simulations³¹⁻³⁴. In particular, this is the first experimental observation of B_{\perp} - and B_{\parallel} -driven QGS of SMT in a 3D anisotropic superconductor and in an unconventional high- T_c superconductor, which serves to catalyze new research efforts on substantially extended physical grounds of the QGS effect.

Magnetic-field-driven SMTs with multiple QCPs in CaFe_{1-x}Ni_xAsF single crystals

High quality CaFe_{1-x}Ni_xAsF single crystals were synthesized and characterized as shown in Methods and Supplementary Information S1&S2. For clarity, CaFe_{1-x}Ni_xAsF samples with $x = 3.1\%$, 3.5% , 3.7% and 4.9% are denoted as sample A, B, C and D, respectively. Figs. 1a-d show the resistance versus temperature $R(T)$ curves of samples A-D under both B_{\perp} (upper panels) and B_{\parallel} (lower panels) from 0 T to 14 T in log-log scale. The $R(T)$ curves in linear coordinates are shown in Supplementary Information S4. The onset superconducting transition temperature at zero field (T_c^{onset}) for sample A, B, C and D are 5.75 K, 6.3 K, 7.5 K and 11 K, respectively. The upper panels of Figs. 1a-d show monotonically decreasing superconducting transition temperature T_c with increasing B_{\perp} , ultimately leading to a weakly insulating $R(T)$ without superconducting transition at arbitrarily low temperatures, i.e., leading to a B_{\perp} -driven SMT. The lower panels of Figs. 1a-d show similar monotonic decrease in T_c with increasing B_{\parallel} , but the B_{\parallel} -driven SMT is only observed in sample A (Fig. 1a, lower panel). For samples B, C and D (Figs. 1b-d, lower

panels), it is evident that $B_{//}$ larger than 14T may be required to fully suppress superconductivity and to achieve SMT. The brown arrows in Figs. 1a-d highlight the $R(T)$ curves at specific “critical” magnetic fields where no onset of superconductivity can be detected at the lowest measured temperature, representing the emergence of magnetic field-driven SMT in each sample. Below these critical magnetic fields, continuously changing crossing points in the $R(B)$ isotherms can be extracted from the $R(T, B)$ data (see Fig. 3), indicative of the presence of multiple QCPs and contrasts with conventional quantum phase transitions with a single QCP^{2,8,9}.

Doping tunable quasi-2D to 3D anisotropic crossover in $\text{CaFe}_{1-x}\text{Ni}_x\text{AsF}$ single crystals

Electronic dimension is an important character that governs material properties and detectable via transport techniques. Here we show that Ni doping can induce an electronic dimensional crossover in the $\text{CaFe}_{1-x}\text{Ni}_x\text{AsF}$ single crystals. Among the four samples investigated in this study, sample A has 3D anisotropic electronic structure while samples B, C and D have quasi-2D electronic structures, in both the normal states and the superconducting states. We shall focus on samples A and C in the main text; data from samples B and D can be found in Supplementary Information S5-8. Figs. 2a-b show the normal state magnetotransport data MR vs. $B\cos\theta$ for samples A and C, respectively. Here, the magnetic field ranges from 0 T to 14 T with its angle θ from 0° (along the c -axis) to 90° (along the a -axis, defined as the in-plane direction perpendicular to the current) and the temperature $T = 14 \text{ K} > T_c$. As shown in Fig. 2a, the MR curves of sample A do not scale into a single curve when plotted with $B\cos\theta$, pointing to a three-dimensional Fermi surface in the normal state of sample A. On the contrary, the MR curves of sample C scale remarkably well with $B\cos\theta$ (Fig. 2b), indicating the dominance of two-dimensional Fermi surface in sample C above T_c [35,36]. For the superconducting state, Figs. 2c-d show the angular dependence of the upper critical field (H_{c2}) at $T = 1.58 \text{ K} < T_c$ for sample A and C, respectively. Here, H_{c2} is defined as the magnetic field where the resistance becomes 50% of the normal state resistance, which is extracted from Supplementary Information S13 and S9 for sample A and C, respectively. In Fig. 2c, $H_{c2}(\theta)$ of sample A can be well fitted by the 3D anisotropic mass model³⁷, where $H_{c2}(\theta) = H_{c2}^{//} / (\sin^2 \theta + \gamma^2 \cos^2 \theta)^{1/2}$ with $\gamma = H_{c2}^{//} / H_{c2}^\perp$, but not the 2D Tinkham model³⁸, where $(H_{c2}(\theta) \sin \theta / H_{c2}^{//})^2 + |H_{c2}(\theta) \cos \theta / H_{c2}^\perp| = 1$, indicating that the superconducting state in

sample A is still three-dimensional. Here H_{c2}^{\parallel} and H_{c2}^{\perp} represent the in-plane and out-of-plane upper critical field, respectively. In contrast, Fig. 2d shows the $H_{c2}(\theta)$ of sample C that can be fitted by the 2D Tinkham model but not the 3D anisotropic mass model; together with the Berezinskii–Kosterlitz–Thouless (BKT) transition³⁹ observed in sample C (Supplementary Information S10), it is evident that sample C has a quasi-2D superconducting electronic state. Similar analysis is performed for sample B and D as shown in Supplementary Information S5a and S7a, respectively, also showing quasi-2D electronic structure for the two samples.

QGS in quasi-2D and 3D anisotropic unconventional high- T_c SCs

Since QGS has so far been observed in 2D and quasi-1D conventional superconductors, we first investigate the possibility of QGS states in quasi-2D unconventional high- T_c SCs (Sample B, C and D). Fig. 3a shows the MR of sample C versus B_{\perp} at various temperatures ranging from 0.46 K to 7 K. Indeed, the MR isotherms exhibit a series of continuously moving crossing points (B_c , R_c) rather than a single point, indicative of QGS behavior. Fig. 3b plots the evolution of the line of "critical" points for the SMTs in terms of B_c versus T . Notably, as T decreases, B_c exhibits continuous upward displacement, deviating from the mean field Werthamer-Helfand-Hohenberg (WHH) theory⁴⁰, in agreement with previous reports in 2D QGS of SMTs in conventional superconductors^{17,18}.

To gain a quantitative understanding of the QGS in $\text{CaFe}_{1-x}\text{Ni}_x\text{AsF}$ samples, we employed finite-size scaling (FSS) analysis to investigate the critical points of the SMTs. The resistance of the sample near these critical points follows a scaling form¹: $R(\delta, t) = R_c \cdot f[\delta \cdot t(T)]$. Here, $t \equiv (T/T_0)^{-1/z\nu}$ with z the dynamical critical exponent, ν the correlation length exponent and T_0 the lowest temperature in the fitting range; R_c and B_c are the critical resistance and critical magnetic field obtained from the critical points, respectively; $\delta = |B - B_c|$ is the deviation from B_c and $f(x)$ is an arbitrary function with $f(0) = 1$. For the quasi-2D sample C, the "critical" point (B_c , R_c) of a certain small critical transition region is defined as the crossing point of several $R(B)$ curves with adjacent temperatures (details in Supplementary Information S11). The scaling results are presented in Supplementary Information S12 and Fig. 3c, which give the effective "critical"

exponents $z\nu$ versus T and B , respectively. Supplementary Information S12 shows that $z\nu$ diverges with decreasing temperature, indicating an enhanced effect of the quenched disorder, which introduces locally ordered superconducting rare regions on the microscopic level^{5,14,15}. Fig. 3c displays $z\nu$ vs. B , which are found to follow the activated scaling law $z\nu = C|B_c^* - B|^{-\nu\psi}$. Here C is a constant, $\nu\psi = 0.6$ is the 2D infinite-randomness critical exponent and $B_c^* = 7.9\text{T}$ is the divergent critical field, as obtained from the fitting. The value of $\nu\psi$ in 2D systems with infinite-randomness are predicted to be ~ 0.6 ($\nu \approx 1.2$ and $\psi \approx 0.5$)^{33,34}, which agrees well with our experiment, providing strong evidence for the existence of QGS in quasi-2D sample C. Additional data on QGS in other quasi-2D samples B and D are presented in Supplementary Information S5-8. We note that most of the Fe-based and Cu-based high- T_c superconductors exhibit only one QCP in their SMT/SIT^{2,8}, with the only exception of underdoped $\text{La}_{2-x}\text{Sr}_x\text{CuO}_4$ films that exhibit two QCPs⁴. Thus, our data represents the first discovery of quasi-2D unconventional high- T_c superconductors to host QGS in their superconductor-metal quantum phase transitions.

Despite the fact that QGS is rarely found in quasi-2D unconventional high- T_c superconductors, QGS in 3D superconducting systems is even more elusive due to experimental and theoretical difficulties⁴¹. Fig. 3d shows MR of 3D anisotropic sample A versus B_\perp at temperatures ranging from 0.49 K to 5.75 K; MR versus B_\parallel of sample A can be found in Supplementary Information S14. Surprisingly, the MR isotherms exhibit continuous movement of crossing points as sample temperature changes, indicative of QGS behavior of sample A under both B_\perp and B_\parallel . Fig. 3e and the inset of Supplementary Information S14b show B_c versus T for B_\perp and B_\parallel configurations, respectively, which show similar deviation from the WHH theory at the low T regime. FSS analysis is carried out for data collected from 3D anisotropic sample A (details in Supplementary Information S15-S16). Fig. 3f shows the resulting $z\nu$ vs. B_\perp curve for sample A, following the same activated scaling law with $B_{c\perp}^* = 4.07\text{ T}$ and $\nu\psi \approx 0.4$. Numerical simulations of 3D random quantum magnets^{31,32} have predicted a correlation length exponent $\nu \approx 0.98$ and a tunneling critical exponent $\psi \approx 0.46$, resulting in $\nu\psi \approx 0.45$, in close agreement with our experiment. The analysis of $z\nu$ vs. B_\parallel for sample A can be found in Supplementary Information S14b. The critical behavior of

sample A under B_{\perp} and B_{\parallel} is found to have only two differences: 1) B_c under B_{\perp} diverges with decreasing temperature at the low- T limit, while B_c under B_{\parallel} appears to saturate at low temperatures. This phenomenon will be discussed in details in the Discussion Section. 2) the B_c^* for the diverging $z\nu$ is 4.07 T for B_{\perp} (Fig. 3f) and 12.41 T for B_{\parallel} (Supplementary Information S14b), highlighting the weakly anisotropic nature of the 3D electronic structure of sample A. Apart from these two differences, the behavior of sample A under B_{\perp} and B_{\parallel} is essentially the same, including the fitted critical exponents $\nu\nu \approx 0.4$, which are both in agreement with numerical simulations^{31,32}. This remarkable consistency between the experimental data and the numerical simulations provides compelling evidence for the presence of QGS in the 3D unconventional high- T_c superconductor $\text{CaFe}_{1-x}\text{Ni}_x\text{AsF}$ ($x = 3.1\%$), representing the first experimental demonstration of magnetic field driven QGS of SMT in 3D systems.

***B-T* phase diagram and discussions**

Based on data from sample A, B - T phase diagrams of bulk 3D anisotropic unconventional Fe-based superconducting system with QGS under B_{\perp} (Fig. 4a) and B_{\parallel} (Fig. 4b) are constructed. The phase diagrams are characterized by three curves: 1) the superconducting onset T_c^{onset} vs. B curve (purple squares) which coincides with the B_c vs. T curve (orange dots); 2) the mean field WHH⁴⁰ upper critical field B_{c2}^{fit} vs. T curve (red dashed line); 3) the upper critical field H_{c2} vs. T curve (blue dots, extracted from 90% of the normal resistance). These three curves divide the phase diagram into four regions: the SC state, the fluctuation region (including ‘‘QF’’: quantum fluctuations and ‘‘TF’’: thermal fluctuations), the QGS state and the normal state.

As shown in Fig.4a, the normal state in the diagram behaves as weakly localized metal above the overlapping points of $T_c^{\text{onset}}(B)$ and $B_c(T)$. The fluctuation region lies between the mean-field B_{c2}^{fit} vs. T curve (red dashed line) and the H_{c2} vs. T curve (blue dashed line). At low T , the $T_c^{\text{onset}}(B)$ curve turns upwards and significantly deviates from the mean-field WHH⁴⁰ behavior below a temperature $T_M \sim 1.9$ K, indicating the emerging quantum fluctuation below T_M ^{21,42}. In particular, for temperatures below T_M and for magnetic field above the mean-field WHH limit⁴⁰, the quantum Griffiths state emerges, characterized by a diverging $z\nu$ and an upturning $B_c(T)$ at

low temperatures⁵. This quantum Griffiths state can be regarded as the effect related to quenched disorder on the Abrikosov vortex lattice in the region of $B_{c2}^{\text{fit}} < B < B_c^*$, where rare regions of large SC puddles appear when $T < T_M$. Meanwhile, the exponentially small excitation energy causes ultraslow dynamics accompanied by diverging effective dynamical exponent around zero T , similar to the behavior of large clusters in the random transverse field Ising model⁴³. It is worth noting that QGS in samples A-D are conspicuously robust¹⁸ (shown in Fig. 4c), with $T_M \sim 1.8$ K in sample A to $T_M \sim 5.3$ K in sample D, the later higher than any reported values in the literature (more details in Supplementary Information S7c), highlighting the peculiarity of QGS in unconventional high- T_c superconductors.

Fig. 4b depicts the B - T phase diagram of the same sample under $B_{//}$, which exhibits behavior similar to that under B_{\perp} , with one key difference: the $T_c^{\text{onset}}(B)$ or $B_c(T)$ under $B_{//}$ saturates at the low- T limit, resulting in a narrow QGS region, compares to a diverging $T_c^{\text{onset}}(B)$ or $B_c(T)$ under B_{\perp} with decreasing T . Saturating $B_c(T)$ has been previously reported in only three superconducting systems, the $B_{//}$ -driven QGS of SMT in few-layer PdTe₂ films²³ and in β -W films²¹, as well as the B_{\perp} -driven QGS of SIT in TiO films¹⁹. The former two cases^{21,23} are considered to be QGS without the formation of vortex glass state, such that the low- T divergent $B_c(T)$ is absent. For the third case, the saturated $B_c(T)$ is attributed to weaker Josephson coupling of the local rare regions in an insulating normal state background¹⁹. In our case, since the resistance of sample A is much less than previous reports of SMT/SIT in QGS^{19,21,23}, a saturating $B_c(T)$ cannot be explained by weaker Josephson coupling¹⁹; the anisotropic nature of the 3D electronic state in the material, on the other hand, might results in the $B_{//}$ -induced rare regions without the emergence of the vortex glass state²³, leading to a saturating $B_c(T)$.

Summary

In summary, 3D quantum Griffiths singularities have been experimentally observed in the superconductor-metal transition of unconventional high- T_c superconductor CaFe_{1-x}Ni_xAsF ($x = 3.1\%$) single crystals. A comprehensive quantum phase diagram for the 3D-QGS of SMT was established, which demonstrates the universality and similarity of QGS in 2D and 3D SC systems.

The robustness of QGS in FeAs-based SCs has also been confirmed. This work opens a new venue for exploring QGS physics in Fe/Cu-based high- T_c superconductors and in 3D superconducting systems.

Methods

Synthesis of $\text{CaFe}_{1-x}\text{Ni}_x\text{AsF}$ single crystals

In this study, single crystals of $\text{CaFe}_{1-x}\text{Ni}_x\text{AsF}$ were synthesized using the CaAs self-flux method. Initially, a mixture of Ca granules and As grains in a 1:1 ratio was heated at 700°C for 10 hours in an evacuated quartz tube to obtain the CaAs precursor. The CaAs precursor was then subjected to a grinding and sintering process, repeated three times to ensure complete mixing and uniformity of CaAs, which is critical for obtaining high-quality single crystals. Subsequently, Fe powder, Ni powder, FeF_2 powder, and the homemade CaAs flux were mixed together in a stoichiometric ratio of 1-x: x: 1:15 ($x = 4\%, 6\%, 8\%, 10\%$), placed in an alumina crucible, and sealed in a quartz tube under vacuum. The sealed quartz tube was then heated at 950°C and 1230°C for 45 hours and 30 hours, respectively, to promote crystal growth. Finally, the tube was cooled down to 850°C at a rate of 2°C/h, followed by quick cooling to room temperature.

Characterization of $\text{CaFe}_{1-x}\text{Ni}_x\text{AsF}$ superconducting single crystals

The $\text{CaFe}_{1-x}\text{Ni}_x\text{AsF}$ crystals exhibited a tetragonal structure, consisting of alternating CaF and $(\text{Fe}_{1-x}\text{Ni}_x)\text{As}$ layers along the c -axis, as depicted in Supplementary Information S1a. A typical high quality $\text{CaFe}_{1-x}\text{Ni}_x\text{AsF}$ single crystal (sample C, $x = 3.7\%$) has rectangular shape and approximately 4 x 3 x 0.15 mm in size, as shown in the inset of Supplementary Information S1b. X-ray diffraction of the $\text{CaFe}_{1-x}\text{Ni}_x\text{AsF}$ crystals (Supplementary Information S1c) confirmed the high crystallinity of the as-grown crystals with (001) orientation, consistent with the parent CaFeAsF compound⁴⁴. Further characterization using scanning electron microscopy and energy dispersive spectrometer analysis (details in Supplementary Information S2) revealed flat as-grown (001) surfaces with definite Ni contents for different crystals. The above results prove the first successful growth of high-quality $\text{CaFe}_{1-x}\text{Ni}_x\text{AsF}$ single crystals.

Transport Measurements

Transport measurements were conducted in the temperature range of 0.3 K to 300 K, under magnetic fields of up to 14 T, using both an Oxford Teslatron cryostat and a Quantum Design PPMS. The resistance was measured at a frequency of 17.77 Hz using conventional lock-in techniques.

Data Availability Statement

Source data are provided with this paper. Data for figures that support the current study are available at doi://xxx.

Acknowledgements

This project has been supported by the National Key R&D Program of China (Grant No. 2019YFA0308402), the Innovation Program for Quantum Science and Technology (Grant No. 2021ZD0302403), the National Natural Science Foundation of China (NSFC Grant Nos. 11934001, 92265106, 11921005), Beijing Municipal Natural Science Foundation (Grant No. JQ20002). J.-H.C. thanks X.C.X. and H. L. for stimulating discussions. J.-H.C. acknowledges technical supports from Peking Nanofab.

Author contributions

J.-H.C. & S.L. conceived the idea; J.-H.C. directed the experiment; S.L., Y.C. & C. C. provide high quality crystals; S.L. fabricated most of the devices and performed the transport measurements; C.T., H.C., X.W., M.C., J.L., Y.F., J.C., Y.Z., Y.S. & T.H. aided in sample preparation and transport measurement; J.-H.C., S.L., C.T., Y.Z. & Y.S. collected and analyzed the data; S.L. & J.-H.C. wrote the manuscript; all authors commented and modified the manuscript.

Corresponding author

Correspondence to Jian-Hao Chen <chenjianhao@pku.edu.cn>

Competing interests

The authors declare no competing interests.

After the submission of this work, we noticed reports of 3D-QGS in conventional three-dimensional MgTi₂O₄ superconducting film [arXiv:2311.06710] and MoTiN

superconducting film [arXiv:2402.01347].

References

- 1 Sondhi, S. L., Girvin, S. M., Carini, J. P. & Shahar, D. Continuous quantum phase transitions. *Rev. Mod. Phys.* **69**, 315–333 (1997).
- 2 Bollinger, A. T. *et al.* Superconductor–insulator transition in $\text{La}_{2-x}\text{SrxCuO}_4$ at the pair quantum resistance. *Nature* **472**, 458–460 (2011).
- 3 Biscaras, J. *et al.* Multiple quantum criticality in a two-dimensional superconductor. *Nat. Mater.* **12**, 542–548 (2013).
- 4 Shi, X., Lin, P. V., Sasagawa, T., Dobrosavljević, V. & Popović, D. Two-stage magnetic-field-tuned superconductor–insulator transition in underdoped $\text{La}_{2-x}\text{SrxCuO}_4$. *Nat. Phys.* **10**, 437–443 (2014).
- 5 Xing, Y. *et al.* Quantum Griffiths singularity of superconductor-metal transition in Ga thin films. *Science* **350**, 542–545 (2015).
- 6 Saito, Y., Nojima, T. & Iwasa, Y. Highly crystalline 2D superconductors. *Nat. Rev. Mater.* **2**, 16094 (2016).
- 7 Zhang, E. *et al.* Signature of quantum Griffiths singularity state in a layered quasi-one-dimensional superconductor. *Nat. Commun.* **9**, 4656 (2018).
- 8 Schneider, R., Zaitsev, A. G., Fuchs, D. & H, V. L. Superconductor-insulator quantum phase transition in disordered FeSe thin films. *Phys. Rev. Lett.* **108**, 257003 (2012).
- 9 Böttcher, C. G. L. *et al.* Superconducting, insulating and anomalous metallic regimes in a gated two-dimensional semiconductor–superconductor array. *Nat. Phys.* **14**, 1138–1144 (2018).
- 10 Fisher, M. P. Quantum phase transitions in disordered two-dimensional superconductors. *Phys. Rev. Lett.* **65**, 923–926 (1990).
- 11 Fisher, M. P. A., Grinstein, G. & Girvin, S. M. Presence of quantum diffusion in two dimensions: Universal resistance at the superconductor-insulator transition. *Phys. Rev. Lett.* **64**, 587–590 (1990).
- 12 Griffiths, R. B. Nonanalytic Behavior Above the Critical Point in a Random Ising Ferromagnet. *Phys. Rev. Lett.* **23**, 17–19 (1969).
- 13 Pich, C., Young, A., Rieger, H. & Kawashima, N. Critical behavior and Griffiths-McCoy singularities in the two-dimensional random quantum Ising ferromagnet. *Phys. Rev. B* **81**, 5916–5919 (1998).
- 14 Motrunich, O., Mau, S.-C. & Huse, D. A. Infinite-randomness quantum Ising critical fixed point. *Phys. Rev. B* **61**, 1160–1172 (2000).
- 15 Vojta, T. Rare region effects at classical, quantum and nonequilibrium phase transitions. *J. Phys. A* **39**, R143–R205 (2006).
- 16 Vojta, T. Quantum Griffiths Effects and Smeared Phase Transitions in Metals: Theory and Experiment. *J. Low Temp. Phys.* **161**, 299–323 (2010).
- 17 Xing, Y. *et al.* Ising Superconductivity and Quantum Phase Transition in Macro-Size Monolayer NbSe. *Nano. Lett.* **17**, 6802–6807 (2017).
- 18 Saito, Y., Nojima, T. & Iwasa, Y. Quantum phase transitions in highly crystalline two-dimensional superconductors. *Nat. Commun.* **9**, 778 (2018).
- 19 Zhang, C. *et al.* Quantum Griffiths singularities in TiO superconducting thin films with

- insulating normal states. *Npg Asia Mater* **11** (2019).
- 20 Han, X. *et al.* Disorder-Induced Quantum Griffiths Singularity Revealed in an Artificial 2D Superconducting System. *Adv. Sci.* **7**, 1902849 (2020).
- 21 Huang, C. *et al.* Observation of thickness-tuned universality class in superconducting beta-W thin films. *Sci. Bull.* **66**, 1830-1838 (2021).
- 22 Ji, H., Liu, H., Jiang, H. & Xie, X. C. Disorder effects on quantum transport and quantum phase transition in low-dimensional superconducting and topological systems. *Adv. Phys. X* **6**, 1884133 (2021).
- 23 Liu, Y. *et al.* Observation of In-Plane Quantum Griffiths Singularity in Two-Dimensional Crystalline Superconductors. *Phys. Rev. Lett.* **127**, 137001 (2021).
- 24 Stewart, G. R. Superconductivity in iron compounds. *Rev. Mod. Phys.* **83**, 1589-1652 (2011).
- 25 Terashima, T. *et al.* Fermi Surface with Dirac Fermions in CaFeAsF Determined via Quantum Oscillation Measurements. *Phys. Rev. X* **8**, 011014 (2018).
- 26 Ma, X. *et al.* Correlation-corrected band topology and topological surface states in iron-based superconductors. *Phys. Rev. B* **106**, 115114 (2022).
- 27 Zhang, M. *et al.* Efficient charge carriers induced by extra outer-shell electrons in iron-pnictides: a comparison between Ni- and Co-doped CaFeAsF. *New J. Phys.* **12**, 083050 (2010).
- 28 Gao, B., Ma, Y., Mu, G. & Xiao, H. Pressure-induced superconductivity in parent CaFeAsF single crystals. *Phys. Rev. B* **97**, 174505 (2018).
- 29 Ma, Y. *et al.* Magnetic-field-induced metal-insulator quantum phase transition in CaFeAsF near the quantum limit. *Sci. China Phys. Mech.* **61**, 127408 (2018).
- 30 Fisher, D. S. Random transverse field Ising spin chains. *Phys. Rev. Lett.* **69**, 534-537 (1992).
- 31 Kovács, I. A. & Iglói, F. Infinite-disorder scaling of random quantum magnets in three and higher dimensions. *Phys. Rev. B* **83**, 174207 (2011).
- 32 Kovacs, I. A. & Iglói, F. Renormalization group study of random quantum magnets. *J Phys Condens Matter* **23**, 404204 (2011).
- 33 Vojta, T., Farquhar, A. & Mast, J. Infinite-randomness critical point in the two-dimensional disordered contact process. *Phys. Rev. E* **79**, 011111 (2009).
- 34 Kovács, I. A. & Iglói, F. Renormalization group study of the two-dimensional random transverse-field Ising model. *Phys. Rev. B* **82**, 054437 (2010).
- 35 Sun, Y., Yamada, T., Pyon, S. & Tamegai, T. Structural-transition-induced quasi-two-dimensional Fermi surface in FeSe. *Phys. Rev. B* **94**, 134505 (2016).
- 36 Grigoriev, P. D. Angular dependence of the Fermi surface cross-section area and magnetoresistance in quasi-two-dimensional metals. *Phys. Rev. B* **81**, 205122 (2010).
- 37 Tinkham, M. *Introduction to Superconductivity*, (McGraw-Hill, New York) (1996).
- 38 Tinkham, M. Effect of Fluxoid Quantization on Transitions of Superconducting Films. *Phys. Rev.* **129**, 2413-2422 (1963).
- 39 Halperin, B. I. & Nelson, D. R. Resistive transition in superconducting films. *J. Low Temp. Phys.* **36**, 599-616 (1979).
- 40 Werthamer, N. R., Helfand, E. & Hohenberg, P. C. Temperature and Purity Dependence of the Superconducting Critical Field, H_{c2} . III. Electron Spin and Spin-Orbit Effects. *Phys. Rev.* **147**, 295-302 (1966).
- 41 Zhao, P.-L., Lu, H.-Z. & Xie, X. C. Theory for Magnetic-Field-Driven 3D Metal-Insulator

- Transitions in the Quantum Limit. *Phys. Rev. Lett.* **127**, 046602 (2021).
- 42 Galitski, V. M. & Larkin, A. I. Disorder and Quantum Fluctuations in Superconducting Films
in Strong Magnetic Fields. *Phys. Rev. Lett.* **87**, 087001 (2001).
- 43 Vojta, T. Rare region effects at classical, quantum and nonequilibrium phase transitions.
Journal of Physics A: Mathematical and General **39**, R143-R205 (2006).
- 44 Ma, Y. *et al.* Growth and characterization of millimeter-sized single crystals of CaFeAsF.
Supercond. Sci. Tech. **28**, 085008 (2015).
- 45 Ma, Y. *et al.* Superconductor-Metal Quantum Transition at the EuO/KTaO₃ Interface. *Chin.*
Phys. Lett. **37** (2020).
- 46 Kaur, S. *et al.* Temperature dependent cloaking of the Quantum Griffiths Singularity in
LaScO₃/SrTiO₃ heterostructures. *Preprint at* <https://doi.org/10.48550/arXiv.2206.10215>
(2022).
- 47 Shen, S. *et al.* Observation of quantum Griffiths singularity and ferromagnetism at the
superconducting LaAlO₃/SrTiO₃(110) interface. *Phys. Rev. B* **94** (2016).
- 48 Wang, X. *et al.* Robust quantum Griffiths singularity above 1.5 K in nitride thin films. *Phys.*
Rev. B **107** (2023).
- 49 Xing, Y. *et al.* Quantum Griffiths singularity in two-dimensional superconducting 4H_a-TaSe₂
nanodevices. *Nano Research* **16**, 12281-12285 (2023).

Figures

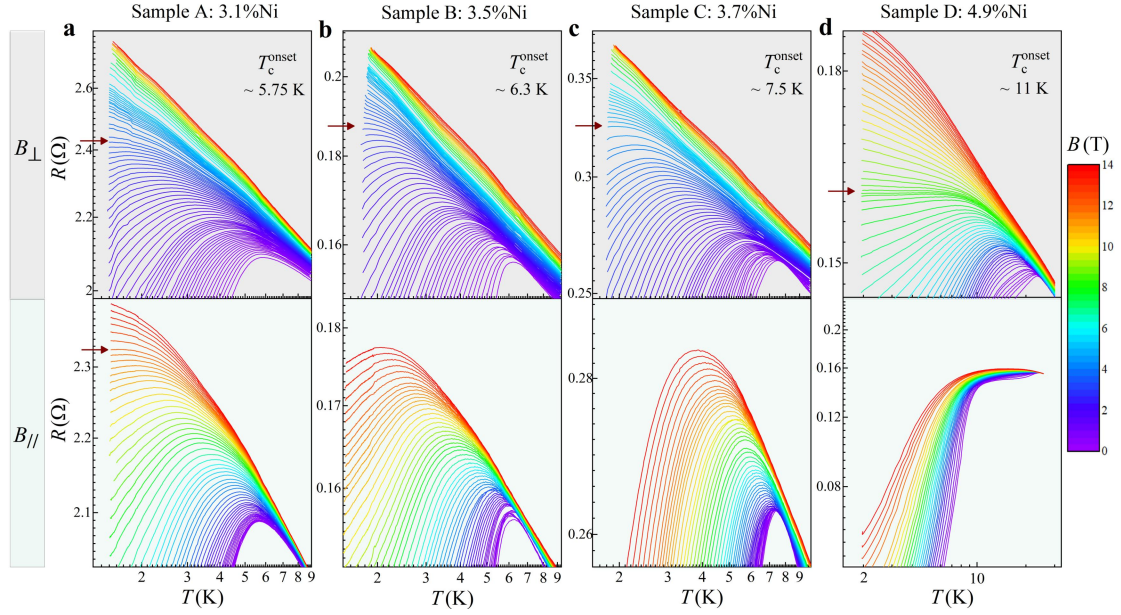


Fig. 1. Magnetic-field-driven SMT with multiple QCPs in $\text{CaFe}_{1-x}\text{Ni}_x\text{AsF}$. a-d, Temperature-dependent resistance under B_{\perp} (upper panels) and B_{\parallel} (lower panels) from 0 to 14 T for $\text{CaFe}_{1-x}\text{Ni}_x\text{AsF}$ samples A, B, C and D in log-log scale, respectively. Different colors represent different magnetic field values. The nickel (Ni) contents and the onset superconducting transition temperature for each sample are marked near the top of the figures. The brown arrows indicate the magnetic field where the field tunable SMTs occur.

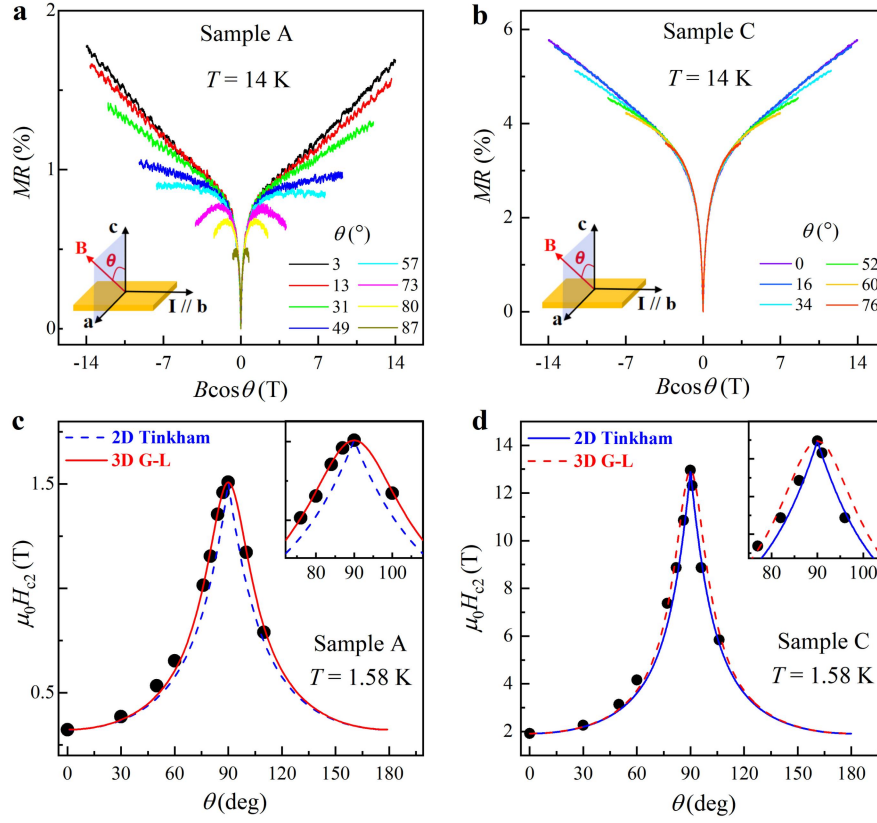


Fig. 2. Doping tunable 3D anisotropic to quasi-2D crossover in CaFe_{1-x}Ni_xAsF single crystals. **a,b**, Normal state MR vs. perpendicular magnetic field $B\cos\theta$ for sample A and C at 14 K, respectively. The magnetic field angle θ , defined in the insets, have values 3° , 13° , 31° , 49° , 57° , 73° , 80° and 87° for sample A and 0° , 16° , 34° , 52° , 60° and 76° for sample C. **c,d**, Angular dependence of the upper critical fields $\mu_0 H_{c2}$ for sample A and C, respectively. The blue and red dashed lines are the theoretical curves of $H_{c2}(\theta)$ from the 2D Tinkham model³⁸ and the 3D anisotropic mass model³⁷, respectively. Insets show the zoom-in plot near $\theta = 90^\circ$. H_{c2} is defined as the magnetic field where the resistance becomes 50% of the normal state resistance.

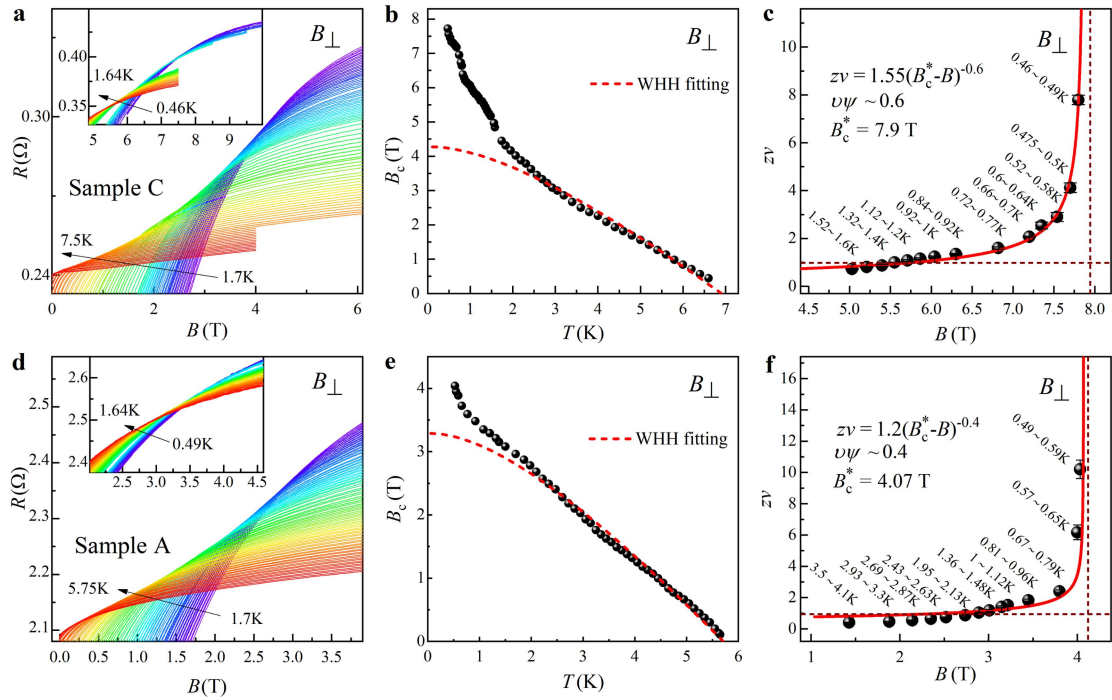


Fig. 3. QGS of SMT in quasi-2D and 3D anisotropic $\text{CaFe}_{1-x}\text{Ni}_x\text{AsF}$ single crystals. a, B_{\perp} dependent resistance isotherms for sample C at $T = 1.7\text{--}7.5$ K in the main panel and $0.46\text{--}1.64$ K in the inset, respectively. b, The critical magnetic field $B_c(T)$ extracted from a, the red dashed line is the fitting curve from the WHH theory⁴⁰. c, The activated quantum scaling behavior of critical exponent $z\nu$ vs. B_{\perp} in sample C. The red solid line is the fitting curve from the activated scaling law and gives $B_c^* = 7.9T$ (vertical dashed line). The horizontal dashed red line shows $z\nu = 1$. d–f, Similar data for sample A as in a–c for sample C under B_{\perp} .

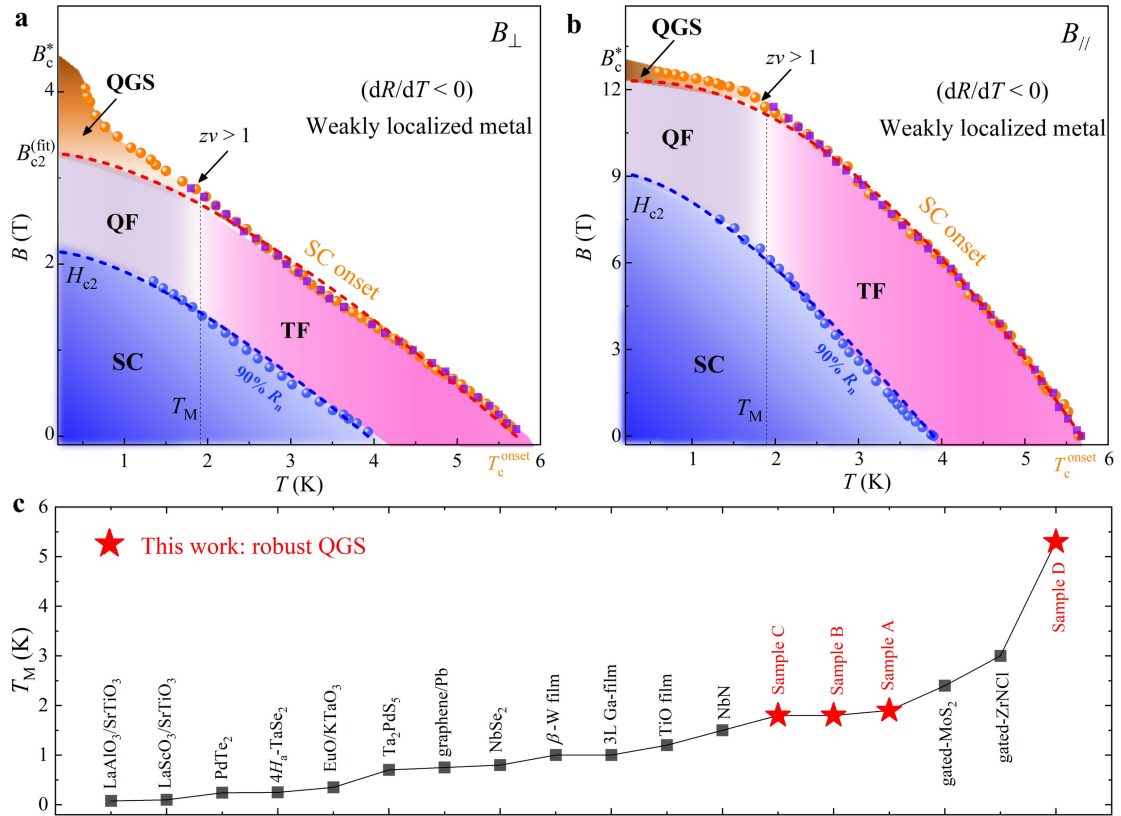


Fig. 4. B - T phase diagram of QGS in a 3D anisotropic superconductor. **a,b,** The phase diagrams are constructed with data from $\text{CaFe}_{1-x}\text{Ni}_x\text{AsF}$ sample A under B_{\perp} and B_{\parallel} , respectively. The QGS phase is the new discovery from this work. Purple squares and orange dots: $T_c^{onset}(B)$ from $R(B)$ vs. T curves and B_c vs. T curves, respectively. Blue dots: H_{c2} vs. T defined as 90% of the normal state resistance. Red and blue dashed lines: fitted curve of $T_c^{onset}(B)$ to the WHH theory⁴⁰. “QF” and “TF” denotes quantum fluctuations and thermal fluctuations, respectively. **c,** Robust QGS in $\text{CaFe}_{1-x}\text{Ni}_x\text{AsF}$ single crystals. We plotted the QGS emerging temperature T_M for sample A, B, C and D together with T_M for all the other reported QGS superconductor-metal transitions in the literature [refs.^{5,7,17-21,23,45-49}]. It can be seen that T_M for $\text{CaFe}_{1-x}\text{Ni}_x\text{AsF}$ single crystals are much higher than other reported values, underscoring the robustness of the QGS in unconventional high- T_c superconductors.